Journal of Applied Physics

# Ion-mediated hopping electrode polarization model for impedance spectra of $CH_3NH_3PbI_3$

Cite as: J. Appl. Phys. **128**, 075104 (2020); https://doi.org/10.1063/5.0020554
Submitted: 02 July 2020 . Accepted: 28 July 2020 . Published Online: 18 August 2020

Osbel Almora, Alfredo González-Lezcano, Antonio Guerrero, Christoph J. Brabec, and Germà Garcia-Belmonte









AIP Publishing

Journal of Applied Physics ARTICLE scitation.org/journal/jap

# Ion-mediated hopping electrode polarization model for impedance spectra of $CH_3NH_3PbI_3$

Cite as: J. Appl. Phys. **128**, 075104 (2020); doi: 10.1063/5.0020554
Submitted: 2 July 2020 · Accepted: 28 July 2020 ·
Published Online: 18 August 2020



Osbel Almora,[1,2,3,a)] Alfredo González-Lezcano,[4,5,6] Antonio Guerrero,[3] Christoph J. Brabec,[1] and Germà Garcia-Belmonte[3]

## AFFILIATIONS

[1]Institute of Materials for Electronics and Energy Technology (i-MEET), Friedrich-Alexander-Universität Erlangen-Nürnberg, 91058 Erlangen, Germany
[2]Erlangen Graduate School in Advanced Optical Technologies (SAOT), Friedrich-Alexander-Universität Erlangen-Nürnberg, 91052 Erlangen, Germany
[3]Institute of Advanced Materials (INAM), Universitat Jaume I, 12006 Castelló, Spain
[4]SISSA International School for Advanced Studies and INFN, 34136 Trieste, Italy
[5]Departamento de Física, Universidad de Pinar del Río, 20100 Pinar del Río, Cuba
[6]The Abdus Salam International Centre for Theoretical Physics, 34014 Trieste, Italy

[a)]**Author to whom correspondence should be addressed:** osbel.almora@fau.de

## ABSTRACT

Methylammonium lead iodide ($CH_3NH_3PbI_3$) is one of the most attractive materials for optoelectronic applications, and it is the most typical absorber in perovskite solar cells, which are unprecedentedly successful devices in terms of power conversion efficiency. In this work, the conductivity and capacitance spectra of symmetrically contacted Au/$CH_3NH_3PbI_3$/Au thick pellets are measured via impedance spectroscopy at different temperatures in dark equilibrium. The experimental conductivity spectra are parameterized and showed to follow the formalism of hopping DC conductivity in the $CH_3NH_3PbI_3$ bulk. The presence of several regimes for the general Jonscher's "universal" conductivity–frequency response is highlighted and associated with the ionic–electronic overlapping conductivities. For the capacitance spectra, the general features of electrode polarization capacitance at the $CH_3NH_3PbI_3$/Au interfaces are identified but yet are found to be in disagreement with some trends of classical ionic conductivity models, unable to separate different contributions. Accordingly, an analytical model is proposed accounting for hopping processes where the low frequency activation energy is split into ionic and electronic components. Our parameterizations and analytical model discern between the bulk/interface and ionic/electronic phenomena and estimate the multiple activation energies in this hybrid halide perovskite.



## I. INTRODUCTION

Methylammonium lead iodide, $CH_3NH_3PbI_3$ (MAPI), has received much attention from the research community since its establishment in 2013 as one of the most promising materials for photovoltaic applications.[1,2] Perovskite solar cells based on MAPI, or similar hybrid halide perovskites, are already able to deliver reproducible power conversion efficiencies above 25% with easy and low cost solution-based fabrication methods.[2–6] Furthermore, the optimal optoelectronic properties of MAPI have also found applications as light-emitting diodes and lasers,[7,8] and several concepts have been proposed for energy storage, such as solar fuels, perovskite batteries, and perovskites in supercapacitors.[9] However, despite the undeniable progress, the understanding of the optoelectronic behavior of this material and devices is still puzzling. In this regard, the impact of the ionic–electronic nature of conductivity is one of the most debated subjects, mostly illustrated in the current–voltage hysteresis phenomena in perovskite solar cells.[10,11]

The electronic conductivity through hopping processes is one of the possible mechanisms that one could consider in polycrystalline semiconductors like solution prepared MAPI. Through this mechanism of quantum nature, the charge carriers hop between

allowed hopping sites with a given energy and position separation. These hops obey given statistics and, as an average, allow net charge carriers to flow.[12] For instance, Slonopas *et al.*[13] proposed Mott variable range hopping conductivity from their analysis of conductivity spectra in MAPI. Moreover, Ambrosio *et al.*[14] did *ab initio* molecular dynamics simulations and found that the localization of the charge carriers and their hopping from one polaronic state to another occur on a sub-picosecond time scale for MAPI. They suggested that the localization is induced by thermal vibrations and only moderately perturbed by the disordered field generated by the organic cations. Furthermore, Yang *et al.*[15] reported hopping rates for different native effects from their density functional theory calculations.

The ionic conductivity in MAPI has been reported in several studies, as summarized by Gregori *et al.*[16] who stressed the long-time/low-frequency effects. The nature of the mobile ions in MAPI has been reviewed by Yuan *et al.*[17] who suggested that both $MA^+$ cations and $I^-$ anions are predominant transport species, while the $Pb_2^+$ ions are more difficult to move. Nevertheless, several subsequent studies have given major importance to iodine vacancies.[18–20] Notably, several authors have calculated dark activation energies around 0.1–1.0 eV for ion conductivity above 250 K, which can be significantly reduced upon illumination.[21–24] The scattering on the reports could be associated with different fabrication methods and measurement conditions/techniques for each sample. More importantly, in all cases, the general assumption is to phenomenologically associate "slow" high temperature phenomena with ions and "fast" response with electronic transport.[25,26] However, an updated theoretical framework has not been provided.

In this article, the conductivity and capacitance spectra of MAPI is presented as a function of temperature via impedance spectroscopy (IS). The frequency and temperature trends are parameterized and correlated with hopping processes joint to ionic conductivity by identifying different conductivity regimes and activation energies. Specifically, an analytical model is presented for explaining the electrode polarization capacitance of MAPI under the effect of hopping conductivity phenomena.

The samples under consideration here were Au/MAPI/Au cylindrical pellets of 1.33 cm diameter, MAPI thicknesses ranging 0.3–1.0 mm, and MAPI crystal sizes as large as 400 $\mu$m. The fabrication details and structural characterization are as described in our previous work.[27] IS measurements were made in a Quatro Cryosystem vacuum chamber ($2.0 \times 10^{-3}$ mbar) with a potentiostat unit from Novocontrol in equilibrium (0 V bias) dark conditions. The equilibrium condition aims to minimize the ion migration into the bulk and electron–hole recombination phenomena. The alternating current (AC) mode perturbation was of 100 mV and the linearity condition was automatically checked at each frequency to be above the 98% of accuracy. The results described below are the most representative among four different samples.

The focus here is set on the conductivity and dielectric properties. From the IS formalism, these are magnitudes mainly related with the real and imaginary parts of the impedance, energy dissipation, and storage.

## II. CONDUCTIVITY AND CAPACITANCE SPECTRA FROM IMPEDANCE SPECTROSCOPY

The direct current (DC) mode conductivity $\sigma_{dc}$ of MAPI has been reported by several authors by means of four probe contact measurements[28] or two electrode contacts, in the DC mode,[29–31] or from the low frequency limit of IS measurements.[23] On the other hand, the AC conductivity has been only described by Sheikh *et al.*[32,33] who identified up to two main regimes at intermediate and higher frequencies, above $\sigma_{dc}$.

The conductivity spectra are shown in Fig. 1(a), with a strong thermal dependency within the tetragonal phase range and up to three power law frequency regimes. The experimental data were parameterized [dots and lines in Fig. 1(a)] to the general Jonscher's "universal" dielectric frequency response,[12,34,35]

$$\sigma = \sigma_{dc}\left(1 + \left(\frac{\omega}{\omega_\sigma}\right)^{\delta}\right), \tag{1}$$

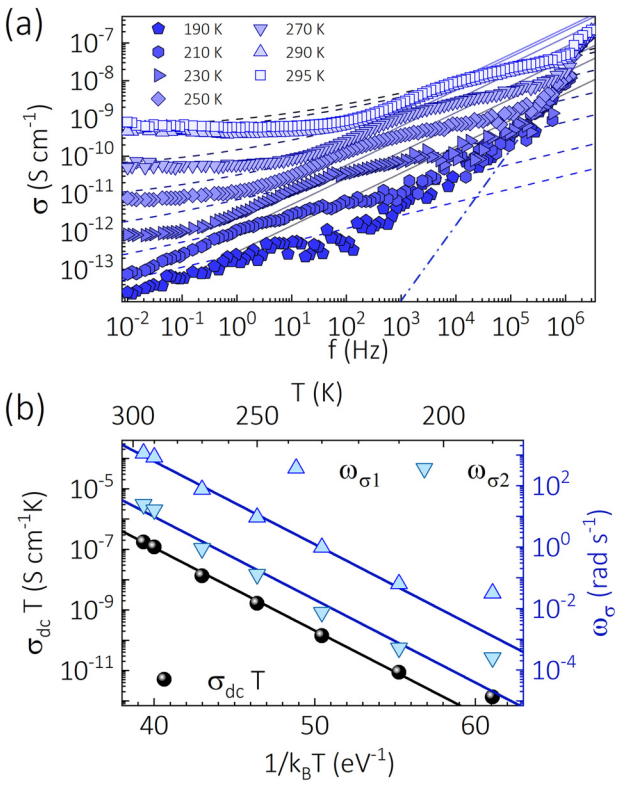


**FIG. 1.** AC conductivity of a MAPI pellet as a function of temperature in a dark equilibrium. (a) Conductivity experimental spectra (dots) and allometric fittings (lines) for each region. (b) Parameterized DC conductivities and respective activation frequencies, left and right axes, respectively, vs temperature (dots), and Arrhenius fitting (lines) with an activation energy $E_\sigma \approx 629$ meV. Adapted with permission from Almora, Ph.D. thesis, Friedrich-Alexander Universität Erlangen-Nürnberg & Universitat Jaume I, 2020. Copyright Author 2020, licensed under a Creative Commons Attribution-NonCommercial-NoDerivs license.

where $\omega_\sigma$ is a characteristic conductivity activation frequency and, well-known in disordered solids,[36–38] the power parameter is predicted to be $0.5 \leq \delta$ by several hopping models[39–42] in ionic conducting glasses, while the diffusion-controlled relaxation model for ionic transport in glasses predicts $0 < \delta < 0.5$.[43] This could correlate the concentrations of mobile ions and hopping sites.

At the lowest frequencies, the DC conductivity in the hopping theory is expected to behave as[35,45]

$$\sigma_{dc} = \frac{Nq^2\lambda_\sigma^2}{6\,k_B T}\omega_\sigma, \tag{2}$$

where $\lambda_\sigma$ is the hopping distance, $N$ is the ionized defect density that establishes the electron concentration, $q$ is the elementary charge, $k_B$ is the Boltzmann constant, $T$ is the temperature, and the effective jump rate $\omega_\sigma$ depends on whether the electron–phonon coupling is strong or weak. In the case of strong coupling,[45]

$$\omega_\sigma = \omega_{\sigma 0}\exp\left[-\frac{E_\sigma}{k_B T}\right], \tag{3}$$

where $\omega_{\sigma 0}$ is the effective attempt-to-jump frequency and $E_\sigma$ is the effective hopping activation energy. The latter parameter is composed at the same time by several contributions as the energy difference between hopping sites,[45] and the free energies of creation and migration of charge carriers.[35] The fitted $\sigma_{dc}$ values are shown to follow (2) with (3) and $E_\sigma \approx 629$ meV in Fig. 1(b). Note that this activation energy approaches theoretical predictions for methylammonium vacancies.[15] Other similar analyses on $\sigma_{dc}$ in MAPI have shown $E_\sigma$ in the range 390–430 meV,[23,29] which most likely relates with iodide vacancies and/or interstitial methylammonium.[15]

At the largest frequencies, the conductivity spectra seem to converge to $\delta = 2$, presented with dotted–dashed lines in Fig. 1(a). At intermediate and lower frequencies, the conductivity behaves as $\delta_2 = 0.35$ and $\delta_1 = 0.7$, as illustrated with the dashed and solid lines in Fig. 1(a), respectively. Correspondingly, the activation frequencies $\omega_{\sigma 1}$ and $\omega_{\sigma 2}$ are presented in Fig. 1(f), showing a clear proportionality with $\omega_\sigma$ as (3) with $E_\sigma \approx 629$ meV too. It is then remarked that the correlation between DC conductivity and hopping rate is accomplished.

Importantly, we stress the fact that Eqs. (2) and (3) characterize the dissipative processes associated with hopping DC conductivities and experimentally obtained from the real part of the impedance. This is most likely the electrical response from the MAPI bulk, presumably through the grain boundaries where the higher surface defect concentration may increase both electronic and ionic conductivity, rather than originated within the perovskite crystals. In an alternative approach, one can inspect the displacement currents associated with the ionic charge accumulation at the interfaces[27,46,47] and the electrode polarization response by measuring the capacitance, from the imaginary part of the impedance spectra.

The equilibrium capacitance spectra of a MAPI pellet in the range 190–295 K are shown in Fig. 2(a). At frequencies below 10 Hz, a clear temperature activated process occurs, most likely

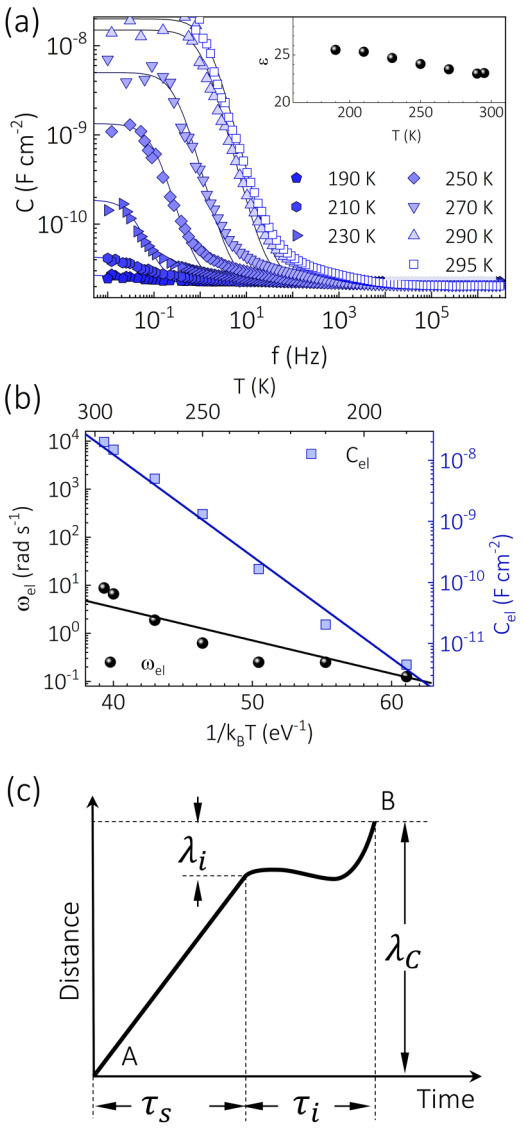


**FIG. 2.** Capacitance of a MAPI pellet as a function of temperature in a dark equilibrium. (a) Capacitance experimental spectra (dots) and fittings (lines) to (4) and (5). The inset in (a) is the dielectric constant behavior with temperature. (b) Activation frequencies and electrode polarization capacitances, in left and right axes, vs temperature (dots), and Arrhenius fittings (lines) with $E_\omega \cong 159$ meV and $E_C \cong 384$ meV, respectively. (c) Schemed drifting–hopping processes of a charge moving from point A to B under AC perturbation in the vicinity to the electrodes. (a) and (b) adapted with permission from Almora, Ph.D. thesis, Friedrich-Alexander Universität Erlangen-Nürnberg & Universitat Jaume I, 2020. Copyright Author 2020, licensed under a Creative Commons Attribution-NonCommercial-NoDerivs license.

related with electrode polarization. The experimental data [dots in Fig. 1(c)] were fitted to

$$C = C_g + C_{\omega T}, \tag{4}$$

where $C_g$ is the geometrical capacitance,[48] nearly frequency independent above 1 kHz, and for lower frequencies,

$$C_{\omega T} = C_{el}\left(1 + \left(\frac{\omega}{\omega_{el}}\right)^2\right)^{-1}, \quad (5)$$

where $C_{el}$ is the electrode polarization capacitance, $\omega_{el}$ is a characteristic activation frequency, and $\omega$ is the angular frequency of the voltage perturbation $\tilde{V} = V_0 \exp[-i\omega t]$ in time $t$ with an amplitude $V_0$ ($i$ is the imaginary unit).

$C_g$ is one of the most basic signals that can be recorded from a single material between symmetric electrodes. Thus, the relative permittivity $\varepsilon = C_g L/\varepsilon_0$ ($\varepsilon_0$ is the vacuum permittivity and $L$ the distance between electrodes) is the main factor to consider at frequencies between 1 kHz and 1 MHz. In this range, nearly frequency-independent plateaus are found with a decrease gradient $\partial\varepsilon/\partial T \sim -0.03\,\mathrm{K}^{-1}$ as the temperature grows [see inset of Fig. 2(a)].

The dielectric function of MAPI has been theoretically obtained from first principles calculations by many authors,[49–58] with a significant scattering between 5 and 38 for the value of the static dielectric constant at room temperature. Experimental analyses have also been reported by means of ultraviolet-visible optical absorption and transmittance spectroscopies,[59,60] spectroscopic ellipsometry, and spectrophotometry.[60–62]

In the tetragonal phase (~160–330 K), Onoda-Yamamuro *et al.*[63] and Mohanty *et al.*[64] measured the static dielectric constant at 1 MHz by IS vs temperature with $\varepsilon \sim 60 - 120$ and thermal gradients $\partial\varepsilon/\partial T \sim -0.3\,\mathrm{K}^{-1}$. At room temperature, Ding *et al.*[30] showed $\varepsilon$ spectrum above 50 too. At 20 kHz, Fabini *et al.*[65] obtained $\varepsilon \sim 35 - 50$. In a range of 40 K above room condition, Yang *et al.*[23] found $\varepsilon \sim 31 - 34$, with $\partial\varepsilon/\partial T \sim -0.05\,\mathrm{K}^{-1}$. Anomalously, Slonopas *et al.*[66,67] found $\varepsilon \sim 10^4$ in a wide plateau spectra between 10 Hz and 100 kHz and in the range 100–350 K.

For the frequency and temperature dependent behavior below 1 kHz, Eq. (5) resembles the Beamount–Jacobs electrode polarization model (BJEPM),[68,69] and the Maxwell–Wagner–Sillars interfacial polarization model[66,67,70] has also been suggested. Less predominant power laws cannot be neglected, but from the Arrhenius of Fig. 1(c), it looks that $C_{el} \propto \exp[-E_C/k_B T]$ with $E_C \cong 384$ meV and $\omega_{el} \propto \exp[-E_\omega/k_B T]$ with $E_\omega \cong 159$ meV.

In the BJEPM,[68,69] only negative carriers are assumed to be mobile and generation/recombination rates are neglected. In principle, one could assume the same in the situation of Fig. 2. However, despite the frequency dependency in the BJEPM is that of (5), the temperature behavior in our experiments [see Fig. 2(b)] is not captured well by this model. Then, the idea is to attack the problem from a different point of view, modifying as little as possible the assumptions that permitted a simplified enough analysis.[68,69]

## III. ANALYTICAL MODEL FOR ELECTRODE POLARIZATION

A theoretical model that reproduces the frequency and temperature behaviors of low frequency capacitance in MAPI pellets will be presented as follows. The good agreement between experimental conductivity spectra and $\sigma_{dc}$ as (2) suggests that the transport of charges could be controlled by discontinuous hopping of charges between localized sites distributed randomly in space and energy. Considering the ionic–electronic conductivity of MAPI and the presumably low bulk defect density of the pellets, the large low frequency capacitance steps in the spectra of Fig. 2 suggest a close interplay between slow ionic phenomena and faster electron conductivity. Thus, one would expect at least two main components in the kinetics of the electrode polarization.

Our model is based on studying the dynamics of charges undergoing a hopping process characterized by the frequency (6), taking also into consideration the time the effective charge moves between hopping events. The two contributions to the charge carrier kinetics toward the electrodes are schemed in Fig. 2(c). For an effective charge carrier moving from point A to B, one first can contemplate a process following the formalism of the Drude–Lorenz model (DLM) of conductivity.[71–73] In the DLM, a set of free moving charges is considered to interact only through collisions with ionic centers. In contrast, our model considers that the interaction of the charges takes place only with the sites over which the charges hop while moving during a time $\tau_s = 2\pi/\omega_s$. This "time of flight" between hopping events may depend on how far apart the two sites are in space and the corresponding thermal fluctuations. Assuming a Boltzmann distribution, the corresponding hopping site capture rate would be

$$\omega_s = \omega_{s0}\exp\left[-\frac{E_s}{k_B T}\right], \quad (6)$$

where $E_s$ is the electronic hopping activation energy that grows linearly with the spatial separation of sites.[12] Subsequently, as an average, the electrons can be trapped in mobile ion-related sites during a time $\tau_i = 2\pi/\omega_i$ and thus hop to another site with a hopping distance $\lambda_i$. This is the schemed point B in Fig. 2(c). Alternatively, one can just consider that the competing effects of electron and ionic transport include an additional characteristic frequency, which can also be assumed to follow a Boltzmann distribution,

$$\omega_i = \omega_{i0}\exp\left[-\frac{E_i}{k_B T}\right]. \quad (7)$$

Here, $E_i$ is an activation energy associated with ionic conductivity and/or how energetically deep is the site in which an electronic charge can be trapped for a time $\tau_i$. Consequently, one can use Ohm's law to relate a component of the imaginary part of the conductivity to the flow of charges near the electrodes under the AC electric field $\tilde{\xi} \cong \tilde{V}/L$, resulting in the displacement current density,

$$J_{el} = N_{el} q v_{eff} = \mathrm{Re}[\omega C_{\omega T} V_0 \exp[-i\omega t]], \quad (8)$$

where $N_{el}$ is the effective charge carrier density, $v_{eff}$ is the effective velocity of the charge carriers that consecutively hop between sites, and $V_0$ is the AC amplitude of the perturbation. Note that the

proper operations in (8) result in

$$J_{el} = \omega C_{\omega T} V_0 \sin[\omega t]. \tag{9}$$

Considering the average time $\tau_s + \tau_i$ needed for an effective charge carrier to move a distance $\lambda_C$ between points A and B, as in Fig. 2(c), the effective charge carrier velocity can be expressed as

$$v_{eff} = v \frac{\omega_i}{\omega_s} \left(1 + \frac{\omega_i}{\omega_s}\right)^{-1}, \tag{10}$$

where $v = \lambda_C/\tau_s$. On the other hand, considering the charge carriers with effective mass $m^*$, Newton's equation of motion can be written as

$$\frac{dv}{dt} = \frac{q}{m^*} \frac{V_0}{L} \mathrm{Re}[\exp[-i\omega t]] - v\omega_s. \tag{11}$$

The first term in (11) comes from the electric force acting on the charge. The second term includes the retarding action of the sites on the charge, even without being the charge trapped in any hopping site. The sinusoidal component of the solution to the differential Eq. (11) is of the form

$$v = \frac{q}{m^*} \frac{V_0}{L} \frac{\omega}{\omega_s^2} \sin[\omega t] \left(1 + \left(\frac{\omega}{\omega_s}\right)^2\right)^{-1}. \tag{12}$$

Upon identification of $v$ in (10) and (12), and assuming $\omega_{i0} \leq \omega_{s0}$ and $E_i > 3E_s$, one can manage the expressions (6)–(12) to finally find

$$C_{\omega T} \cong \frac{N_{el} q^2 \omega_{i0}}{m^* L \omega_{s0}^3} \exp\left[-\frac{(E_i - 3E_s)}{k_B T}\right] \left(1 + \left(\frac{\omega}{\omega_s}\right)^2\right)^{-1}. \tag{13}$$

**TABLE I.** Summary of activation energies, their obtention, and interpretation in this work.

| Parameter | Value (meV) | Obtention method | Physical meaning for the activation energies |
|---|---|---|---|
| $E_\sigma$ | 629 | IS experiment $\sigma(f, T)$, Fig. 1 | Bulk/grain boundary electronic conductivity |
| $E_C = E_i - 3E_s$ | 384 | IS experiment $C(f, T)$, Fig. 2 | Electrode low-frequency capacitance |
| $E_s = E_\omega$ | 159 | $E_\omega$ from IS experiment $C(f, T)$ in Fig. 2, and $E_s$ from theoretical model | Electronic hopping between sites toward the electrodes |
| $E_i$ | 861 | Theoretical model | Ionic motion toward the electrodes |

Equaling (13) to (5) results in $\omega_{el} = \omega_s$, making $E_\omega = E_s \cong 159$ meV and

$$C_{el} \cong \frac{N_{el} q^2 \omega_{i0}}{m^* L \omega_{s0}^3} \exp\left[-\frac{(E_i - 3E_s)}{k_B T}\right], \tag{14}$$

where $E_C = E_i - 3E_s$, making $E_i \cong 861$ meV. Interestingly, the latter also approaches some theoretical estimations for activation energies of methylammonium vacancies.[15] Table I summarizes the above discussion regarding each activation energy. Note that from the experiment, we analyzed three different activation energies ($E_\sigma$, $E_C$, and $E_\omega$), and with the model, we propose an interpretation that introduces $E_i$ as a composing element for $E_C$.

Summing up this section, our theoretical model seems to be compatible with the experimental results, thus validating the phenomenological description of the electrical response. Our analyses indicate the behavior of an ionic solid conductor where one can differentiate the activation energies for electronic hopping and ionic electrode polarization phenomena. The analytical model can easily be applied in the future to different materials and/or devices with similar electrical response.

## IV. CONCLUSIONS

The experimental conductivity and capacitance spectra of MAPI pellets at different temperatures provide information on strong thermal activated processes. These behaviors can be interpreted in terms of the hopping conductivity theory of solids in addition to ionic features. The conductivity spectra show several regimes where different Jonscher's power laws suggest the interplay between electronic conductivity and the possible contribution of several ionic species as hopping sites. An activation energy was found as $E_\sigma \approx 629$ meV. On the other hand, the capacitance spectra show a strong thermally activated increase toward lower frequencies that can be explained if hopping phenomena is considered jointly to ionic motion. A hopping-electrode polarization model is proposed by combining the Drude–Lorentz formalism with hopping processes resulting in a good agreement with the experimental frequency and temperature trends. Our results report on ion movement activation energy $E_i \cong 861$ meV in the vicinity of the electrodes, where charge accumulation takes place. In the contact interface, a higher concentration of defects at the grain boundaries may produce hopping events that contribute to the displacement currents characterizing the electrode polarization capacitance.

## ACKNOWLEDGMENTS

O.A. acknowledges the financial support from the VDI/VD Innovation+Technik GmbH (Project-title: PV-ZUM) and the SAOT funded by the German Research Foundation (DFG) in the framework of the German excellence initiative. G.G.-B. acknowledges the financial support from Ministerio de Ciencia e Innovación (Spain) under Project No. PID2019-107348GB-100. C.J.B. gratefully acknowledges the financial support through the "Aufbruch Bayern" initiative of the state of Bavaria (EnCN and "Solar Factory of the Future"), the Bavarian Initiative "Solar Technologies go Hybrid" (SolTech), and the SFB 953 (DFG, Project No. 182849149).

## DATA AVAILABILITY

The data that support the findings of this study are available within the article.

## REFERENCES


[1]N.-G. Park, J. Phys. Chem. Lett. **4**, 2423 (2013).
[2]H. J. Snaith, J. Phys. Chem. Lett. **4**, 3623 (2013).
[3]M. A. Green, E. D. Dunlop, J. Hohl-Ebinger, M. Yoshita, N. Kopidakis, and A. W. Y. Ho-Baillie, Prog. Photovoltaics Res. Appl. **28**, 3 (2020).
[4]NREL's Best Research-Cell Efficiency Chart, 2020, https://www.nrel.gov/pv/cell-efficiency.html. Accessed 08.07.2020.
[5]J. Bisquert, E. J. Juárez-Pérez, and P. V. Kamat, *Hybrid Perovskite Solar Cells: The Genesis and Early Developments 2009-2014* (Fundació Scito, Valencia, 2017).
[6]N. L. Chang, A. W. Yi Ho-Baillie, P. A. Basore, T. L. Young, R. Evans, and R. J. Egan, Prog. Photovoltaics Res. Appl. **25**, 390 (2017).
[7]S. A. Veldhuis, P. P. Boix, N. Yantara, M. Li, T. C. Sum, N. Mathews, and S. G. Mhaisalkar, Adv. Mater. **28**, 6804 (2016).
[8]M. Stylianakis, T. Maksudov, A. Panagiotopoulos, G. Kakavelakis, and K. Petridis, Materials **12**, 859 (2019).
[9]W. Zhang, G. E. Eperon, and H. J. Snaith, Nat. Energy **1**, 16048 (2016).
[10]H.-S. Kim and N.-G. Park, J. Phys. Chem. Lett. **5**, 2927 (2014).
[11]H. J. Snaith, A. Abate, J. M. Ball, G. E. Eperon, T. Leijtens, N. K. Noel, S. D. Stranks, J. T.-W. Wang, K. Wojciechowski, and W. Zhang, J. Phys. Chem. Lett. **5**, 1511 (2014).
[12]R. M. Hill and A. K. Jonscher, J. Non Crystall. Solids **32**, 53 (1979).
[13]A. Slonopas, B. J. Foley, J. J. Choi, and M. C. Gupta, J. Appl. Phys. **119**, 074101 (2016).
[14]F. Ambrosio, J. Wiktor, F. De Angelis, and A. Pasquarello, Energy Environ. Sci. **11**, 101 (2018).
[15]D. Yang, W. Ming, H. Shi, L. Zhang, and M.-H. Du, Chem. Mater. **28**, 4349 (2016).
[16]G. Gregori, T.-Y. Yang, A. Sonocrate, M. Grätzel, and J. Maier, in *Organic-Inorganic Halide Perovskites Photovoltaics: From Fundamentals to Device Architectures*, edited by N.-G. Park, M. Grätzel, and T. Miyasaka (Springer, 2016), p. 107.
[17]Y. Yuan, Q. Wang, and J. Huang, in *Organic-Inorganic Halide Perovskite Photovoltaics: From Fundamentals to Device Architectures*, edited by N.-G. Park, M. Grätzel, and T. Miyasaka (Springer International Publishing, Cham, 2016), p. 137.
[18]A. Senocrate, I. Moudrakovski, G. Y. Kim, T.-Y. Yang, G. Gregori, M. Grätzel, and J. Maier, Angew. Chem. Int. Ed. **56**, 7755 (2017).
[19]C. Li, A. Guerrero, S. Huettner, and J. Bisquert, Nat. Commun. **9**, 5113 (2018).
[20]H. Lee, S. Gaiaschi, P. Chapon, A. Marronnier, H. Lee, J.-C. Vanel, D. Tondelier, J.-E. Bourée, Y. Bonnassieux, and B. Geffroy, ACS Energy Lett. **2**, 943 (2017).
[21]J. Xing, Q. Wang, Q. Dong, Y. Yuan, Y. Fang, and J. Huang, Phys. Chem. Chem. Phys. **18**, 30484 (2016).
[22]Y.-C. Zhao, W.-K. Zhou, X. Zhou, K.-H. Liu, D.-P. Yu, and Q. Zhao, Light Sci. Appl. **6**, e16243 (2017).
[23]T.-Y. Yang, G. Gregori, N. Pellet, M. Grätzel, and J. Maier, Angew. Chem. Int. Ed. **54**, 7905 (2015).
[24]M. N. F. Hoque, M. Yang, Z. Li, N. Islam, X. Pan, K. Zhu, and Z. Fan, ACS Energy Lett. **1**, 142 (2016).
[25]O. Almora, Y. Zhao, X. Du, T. Heumueller, G. J. Matt, G. Garcia-Belmonte, and C. J. Brabec, Nano Energy **75**, 104982 (2020).
[26]O. Almora, M. García-Batlle, and G. Garcia-Belmonte, J. Phys. Chem. Lett. **10**, 3661 (2019).
[27]O. Almora, A. Guerrero, and G. Garcia-Belmonte, Appl. Phys. Lett. **108**, 043903 (2016).
[28]B. Gebremichael, G. Alemu, and G. Tessema Mola, Physica B **514**, 85 (2017).
[29]O. Knop, R. E. Wasylishen, M. A. White, T. S. Cameron, and M. J. M. V. Oort, Can. J. Chem. **68**, 412 (1990).
[30]X.-K. Ding, X.-M. Li, X.-D. Gao, S.-D. Zhang, Y.-D. Huang, and H.-R. Li, Acta Phys. Chim. Sin. **31**, 576 (2015).
[31]D. Głowienka, T. Miruszewski, and J. Szmytkowski, Solid State Sci. **82**, 19 (2018).
[32]M. S. Sheikh, A. P. Sakhya, A. Dutta, and T. P. Sinha, Thin Solid Films **638**, 277 (2017).
[33]M. S. Sheikh, A. P. Sakhya, P. Sadhukhan, A. Dutta, S. Das, and T. P. Sinha, Ferroelectrics **514**, 146 (2017).
[34]A. K. Jonscher, Nature **267**, 673 (1977).
[35]E. F. Hairetdinov, N. F. Uvarov, H. K. Patel, and S. W. Martin, Phys. Rev. B **50**, 13259 (1994).
[36]J. C. Dyre and T. B. Schrøder, Rev. Mod. Phys. **72**, 873 (2000).
[37]S. Elliott, Solid State Ionics **70–71**, 27 (1994).
[38]J. C. Dyre, P. Maass, B. Roling, and D. L. Sidebottom, Rep. Prog. Phys. **72**, 046501 (2009).
[39]M. Pollak and G. E. Pike, Phys. Rev. Lett. **28**, 1449 (1972).
[40]W. K. Lee, J. F. Liu, and A. S. Nowick, Phys. Rev. Lett. **67**, 1559 (1991).
[41]L. Murawski, R. J. Barczyński, and D. Samatowicz, Solid State Ionics **157**, 293 (2003).
[42]A. Mansingh, Bull. Mater. Sci. **2**, 325 (1980).
[43]S. R. Elliott and A. P. Owens, Philos. Mag. B **60**, 777 (1989).
[44]O. Almora, Ph.D. thesis, Friedrich-Alexander Universität Erlangen-Nürnberg & Universitat Jaume I, 2020.
[45]K. Shimakawa, in *Encyclopedia of Materials Science and Technology*, edited by K. H. J. Buschow, R. W. Cahn, M. C. Flemings, B. Ilschner, E. J. Kramer, S. Mahajan, and P. Veyssière (Elsevier, Oxford, 2001), p. 3579.
[46]J. Caram, M. García-Batlle, O. Almora, R. D. Arce, A. Guerrero, and G. Garcia-Belmonte, Appl. Phys. Lett. **116**, 183503 (2020).
[47]O. Almora and G. Garcia-Belmonte, Sol. Energy **189**, 103 (2019).
[48]P. Lopez-Varo, J. A. Jiménez-Tejada, M. García-Rosell, S. Ravishankar, G. Garcia-Belmonte, J. Bisquert, and O. Almora, Adv. Energy Mater. **8**, 1702772 (2018).
[49]F. Brivio, A. B. Walker, and A. Walsh, APL Mater. **1**, 042111 (2013).
[50]F. Brivio, K. T. Butler, A. Walsh, and M. van Schilfgaarde, Phys. Rev. B **89**, 155204 (2014).
[51]J.-S. Park, S. Choi, Y. Yan, Y. Yang, J. M. Luther, S.-H. Wei, P. Parilla, and K. Zhu, J. Phys. Chem. Lett. **6**, 4304 (2015).
[52]D. O. Demchenko, N. Izyumskaya, M. Feneberg, V. Avrutin, Ü. Özgür, R. Goldhahn, and H. Morkoç, Phys. Rev. B **94**, 075206 (2016).
[53]M. Sendner, P. K. Nayak, D. A. Egger, S. Beck, C. Muller, B. Epding, W. Kowalsky, L. Kronik, H. J. Snaith, A. Pucci, and R. Lovrincic, Mater. Horiz. **3**, 613 (2016).
[54]M. Shirayama, H. Kadowaki, T. Miyadera, T. Sugita, M. Tamakoshi, M. Kato, T. Fujiseki, D. Murata, S. Hara, T. N. Murakami, S. Fujimoto, M. Chikamatsu, and H. Fujiwara, Phys. Rev. Appl. **5**, 014012 (2016).
[55]J. Zhou, F. L. Tang, H. T. Xue, and F. J. Si, Mater. Sci. Forum **850**, 245 (2016).
[56]M. A. Pérez-Osorio, A. Champagne, M. Zacharias, G.-M. Rignanese, and F. Giustino, J. Phys. Chem. C **121**, 18459 (2017).
[57]P. Umari, E. Mosconi, and F. De Angelis, J. Phys. Chem. Lett. **9**, 620 (2018).
[58]O. Almora, P. Lopez-Varo, K. T. Cho, S. Aghazada, W. Meng, Y. Hou, C. Echeverría-Arrondo, I. Zimmermann, G. J. Matt, J. A. Jiménez-Tejada, C. J. Brabec, M. K. Nazeeruddin, and G. Garcia-Belmonte, Sol. Energy Mater. Sol. Cells **195**, 291 (2019).
[59]A. Yang, M. Bai, X. Bao, J. Wang, and W. Zhang, J. Nanomed. Nanotechnol. **7**, 407 (2016).
[60]J. A. Guerra, A. Tejada, L. Korte, L. Kegelmann, J. A. Töfflinger, S. Albrecht, B. Rech, and R. Weingärtner, J. Appl. Phys. **121**, 173104 (2017).
[61]P. Löper, M. Stuckelberger, B. Niesen, J. Werner, M. Filipič, S.-J. Moon, J.-H. Yum, M. Topič, S. De Wolf, and C. Ballif, J. Phys. Chem. Lett. **6**, 66 (2015).
[62]C. G. Bailey, G. M. Piana, and P. G. Lagoudakis, J. Phys. Chem. C **123**, 28795 (2019).

[63]N. Onoda-Yamamuro, T. Matsuo, and H. Suga, J. Phys. Chem. Solids **53**, 935 (1992).
[64]A. Mohanty, D. Swain, S. Govinda, T. N. G. Row, and D. D. Sarma, ACS Energy Lett. **4**, 2045 (2019).
[65]D. H. Fabini, T. Hogan, H. A. Evans, C. C. Stoumpos, M. G. Kanatzidis, and R. Seshadri, J. Phys. Chem. Lett. **7**, 376 (2016).
[66]A. Slonopas, B. Kaur, and P. Norris, Appl. Phys. Lett. **110**, 222905 (2017).
[67]A. Slonopas, H. Ryan, and P. Norris, Electrochim. Acta **307**, 334 (2019).
[68]J. H. Beaumont and P. W. M. Jacobs, J. Phys. Chem. Solids **28**, 657 (1967).
[69]C. Kim and M. Tomozawa, J. Am. Ceram. Soc. **59**, 127 (1976).
[70]M. Samet, V. Levchenko, G. Boiteux, G. Seytre, A. Kallel, and A. Serghei, J. Chem. Phys. **142**, 194703 (2015).
[71]P. Drude, Ann. Phys. **306**, 566 (1900).
[72]B. Cichocki and B. U. Felderhof, J. Chem. Phys. **104**, 3013 (1996).
[73]B. Cichocki and B. U. Felderhof, J. Chem. Phys. **107**, 6390 (1997).